Remarkably stable and efficient Ni and Ni-Co catalysts for CO2 methanation

Bachar Alrafei, Isabelle Polaert, Alain Ledoux, Federico Azzolina-Jury

CATTOD_2018_1084- R1

Title: Remarkably stable and efficient Ni and Ni-Co catalysts for CO_2 methanation

Author Names:

Bachar Alrafei [a], Isabelle Polaert [a], Alain Ledoux [a], Federico Azzolina-Jury [b]

[a] Normandie University, INSA Rouen, LSPC, Laboratoire de Sécurité des Procédés Chimiques, EA 4704 - INSA Rouen, Avenue de l'Université – Saint-Étienne-du-Rouvray cedex 76801 France

[b] Normandie University, ENSICAEN, UNICAEN, LCS, Laboratoire Catalyse & Spectrochimie, 14000 Caen, France

Corresponding Author:

Isabelle Polaert

INSA Rouen, LSPC, Laboratoire de Sécurité des Procédés Chimiques, EA 4704 - INSA Rouen, Avenue de l'Université – Saint-Étienne-du-Rouvray cedex 76801 France.

mail address: isabelle.polaert@insa-rouen.fr

Abstract

CO_2 methanation is one of the most promising ways to store energy based on the power-to-gas concept. In this study, efficient nickel (Ni) and nickel-cobalt (Ni-Co), supported on alumina catalysts with different amounts of Ni and Co were prepared, characterized and used for CO_2 methanation under the atmospheric pressure. The catalysts were prepared in the form of extrudates for catalytic tests. The effect of Ni content and the influence of Co on Ni catalysts were studied in a packed bed methanation reactor at laboratory scale. An optimal Ni-Co content was identified based on CO_2 and H_2 conversion and CH_4 selectivity and yield. The addition of Co improved the reducibility of Ni species and Ni particles' dispersion over the support. Therefore, the presence of Co enhanced the catalyst activity and selectivity towards CH_4. Moreover, it was observed that low reaction temperatures (lower than 350 °C) can be used when lowering the Ni content (i.e. 10% wt.). This major fact is favourable to the reduction of the overall process energy consumption and to the decrease of the catalysts' deactivation at high temperature (>400 °C), such as the active phase sintering. Finally, the Ni and Ni-Co catalysts prepared in this work for CO_2 methanation presented a remarkably high stability over 200 h of continuous reaction.

Keywords: Methanation, Ni-Co catalyst, Green process, CO_2 valorisation, Power-to-gas.

1 Introduction

One of the most serious issues in the climate debates and the countries' agreements is focused on the continuous increase in CO_2 emissions. The CO_2 concentration in our atmosphere has already reached 408 ppm in 2018 [1]. CO_2 is the most abundant greenhouse effect gas emitted by the humans activities, representing more than 77% of the greenhouse gas emissions. It contributes to the global warming and climate change [2,3]. Other consequences, such as sea-level rise, resulting from the thermal expansion or melting of glaciers and polar ice caps, and changes in agriculture, water and human health have been reported as well [4]. On this matter, several agreements have been made, for example the Paris Agreement in 2015 at the International Conference on Climate, COP21. Despite the fact that some countries have reneged this commitment, CO_2 emissions control remains a key point for the future and objectives set in those agreements are still needed to be targeted. The main objective is the reduction of earth's

temperature and CO_2 emissions through the promotion of renewable energy sources. European commission has prospected a target of 20% renewable energy by 2020 in its "Energy Roadmap 21" [5]. Recent agreements are pushing the countries for the use of renewable energies alongside the fossil energies, which would be substituted by the renewables at mid-term.

The renewable energy resources, such as wind, solar, hydrothermal and hydraulic energy are converted to electricity, because the transport of energy is the easiest in this form. However, one of the main problems of renewable energy sources is the difficulty of storing the energy produced. Indeed, solar panels or wind turbines allow an intermittent generation of electricity, because of its dependency on the weather; thus, this production cannot fulfil the load demand of the electric energy. One of the major challenges in the coming years is to find large capacities and long term solution to store the surplus electricity. The current storage technologies, including pumped-storage hydroelectricity (PSH)—the most massive storage technology available—can store only limited amounts of energy over short period of time [6].

In this context, hydrogen can be obtained by the electrolysis of water, which can store large quantities of electrical energy in form of hydrogen and oxygen. These two molecules can be used directly or as intermediates in the chemical reactions to either reproduce energy or synthesize chemical products. However, low molecular weight of hydrogen gives it a relatively low volumetric energy density compared to other fuels, and induces necessary large storage capacities at high pressures. In addition, its explosive properties entail drastic safety management. Besides, hydrogen cannot be injected directly into the natural gas grid, because its concentration usually overcomes the grid technical specifications [7].

51 CO_2 methanation uses the hydrogen produced by water electrolysis and CO_2 for further
52 production of methane. The methanation reaction, known as Sabatier reaction, can be written as
53 follows:

$$CO_2 + 4H_2 \longleftrightarrow CH_4 + 2H_2O \qquad \Delta H_{298\,K} = -164\ kJ/mol,\ \Delta G^0 = -113\ kJ/mol \qquad (1)$$

54 Carbon monoxide can be a product in the methanation by reverse water gas shift reaction [8]:

$$CO_2 + H_2 \longleftrightarrow CO + H_2O \qquad \Delta H_{298\,K} = 41\ kJ/mol,\ \Delta G^0 = 28.6\ kJ/mol \qquad (2)$$

55 The Sabatier reaction leads to an improvement in energy density; the energy density of methane
56 is 40 MJ/m^3, while that of hydrogen is just 12.7 MJ/m^3. In terms of greenhouse gas emissions,
57 methane is the major constituent of natural gas, and is the world's third-most-consumed source of
58 energy. It is the cleanest gas among fuels currently being used. In addition, unlike hydrogen,
59 methane has its own distribution infrastructure, which makes it a convenient fuel for modern
60 economies [8]. The existing gas networks provide high storage capacity and possibility to
61 transport methane easily and safely. Methane can then be used for heating, industries or mobility
62 uses.

63 The development of an industrial CO_2 methanation process is still limited despite the discovery of
64 the reaction since more than a century [9]. However, some industrial applications of CO_2
65 methanation already exist, but they are still poorly developed. Many of those processes date back
66 to the '60s and '80s. In these processes, two types of reactors are mainly used: fluidized bed and
67 packed bed reactors. Packed bed reactors are mostly used in industry, because of the ease of
68 setting up and low cost of maintenance. The heat management is mandatory for this sort of
69 reactor. Poor heat transfer could easily be the cause of hot spots generation within the catalytic
70 bed and of catalyst thermal degradation, particularly in the case of exothermic reactions like CO_2

methanation. To manage the thermal issues using packed bed reactors, CO_2 methanation processes usually involve multiple reactors in series separated by heat exchangers. Table 1 shows some of those processes with their operating conditions [8,10,11].

Table 1 : Existing methanation processes

Process / Company	Reactor type	Number of beds	Pressure (bar)	Temperature (°C)
TREMP/Haldor Topsøe (Denmark, Germany)	Fixed bed	3	30	300–700
Hicom/British Gas Corp (UK)	Fixed bed	4	25–70	230–640
RMP/Ralph M. Parsons Co (US)	Fixed bed	4–6	1–70	315–780
SuperMeth, ConoMeth/Conoco (US)	Fixed bed	4	80	-
Hygas/Institute of Gas Technology (US)	Fixed bed	2	70	280–480
Lurgi, Sasol/Lurgi GmbH (US)	Fixed bed	2	18	450
ICI, Koppers/Imperial Chemical industries (UK)	Fixed bed	3	-	400–700
Comflux/Thysengas GmbH (Germany)	Fluidized bed	1	20–60	400–500
Bi-Gas/Bituminous Coal Res. Inc (US)	Fluidized bed	1	86	-

Some recent projects [12,13], such as the Audi e-gas project and the one developed at University of Corsica are in operation since 2013. Other projects are being developed, such as Jupiter 1000, the first French experience in power-to-gas technology at megawatt (MW) level [14].

CO_2 methanation is a volume-reducing and exothermic reaction. As a consequence, it is thermodynamically favoured at low temperature (Van't Hoff) and high pressure (Le Chatellier). CO_2 methanation mechanism implies firstly, the CO_2 dissociation into CO, which has been proposed as reaction intermediate during the last decades. CO is then dissociated into C (and O) atoms on the metallic active sites to be further hydrogenated into methane by combination with the dissociated H_2. The rate-limiting step of the CO_2 methanation reaction is the dissociation of the adsorbed CO into C and O atoms on the metallic sites. The overall reaction rate is slow and

86 considerable attention needs to be paid to develop more efficient catalysts for achieving high
87 reaction rates. However, an efficient catalyst should be able to ensure a good catalytic activity,
88 selectivity, stability and also it should be capable of being recovered and regenerated after use by
89 keeping its initial properties.

90 In the last decades, CO_2 methanation has been extensively investigated on the use of different
91 metals (Ni, Co, Fe, Cu, Ru, Rh, Ir, Pd, Pt) and supports (TiO_2, SiO_2, SiO_2-Al_2O_3, Al_2O_3,
92 $MgAl_2O_4$, MgO, ZrO_2, CeO_2, C, MSN, MCM-41, SBA-15, HY, USY)[15–19]. Group VIIIB
93 metals, such as Rh, Ru, Ni, Co were found to be very active [3,20]. Noble metals present high
94 activity and stability under low temperature [21–23]. They are more resistive to catalyst
95 deactivation (coking and sintering) than other used metals. However, their industrial utilization is
96 avoided because of their high price and low availability. Cobalt (Co) based catalysts were tested
97 on methanation, but they were found to be not very selective towards methane [24]. Most of the
98 studies have come to terms on the use of nickel metal because it is one of the best active metals
99 for the CO_2 methanation, available at a lower price compared to other metals [19]. These
100 properties make its industrial utilization possible. Ni catalysts are active only at high temperature
101 (300–450 °C). At low temperature (lower than 300 °C), the interaction between Ni and CO leads
102 to the formation of subcarbonyls and methanation is inhibited [25]. The activity of a Ni catalyst
103 depends on various parameters, such as support type, preparation method of the catalyst, Ni
104 loading and the presence of a second metal.

105 The nature of the support greatly influences the morphology, dispersion and reducibility of the
106 active phase (metal), and consequently the final properties of the catalyst. Several types of
107 materials can be used as catalytic supports for CO_2 methanation, such as alumina, silica, zeolites,

etc.[19,26]. Alumina is the widely preferred support because of its low price, thermal stability and relatively high surface area.

Table 2 synthetizes some methanation results from the literature, obtained with various Ni-based catalysts supported on oxides. Metal loading is presented as wt%.

Table 2: CO_2 conversion (X_{CO_2}), CH4 selectivity (S_{CH_4}) and yield (Y_{CH_4})

Catalyst	T (°C)	X_{CO_2} (mol%)	S_{CH_4} (mol%)	Y_{CH_4} (mol%)
10%Ni/CeO_2 [27]	340	91	100	91
20%Ni/Al_2O_3 [28]	350	80	100	80
10%Ni/Y_2O_3 [29]	300	80	100	80
23%Ni/CaO-Al_2O_3 [30]	400	81	99	80
15%Ni/ZrO_2 [31]	300	60	100	60
15 %Ni- $Ce_{0.72}Zr_{0.28}O_2$ [32]	350	90	98	88
14%NiUSY [33]	450	65	94	62
60%NiO/SiO_2 [34]	350	86	95	81
15%Ni/TiO_2 [35]	340	80	96	77
10%Ni / Al_2O_3 [36]	400	60	95	57
10%Ni3%Co/ Al_2O_3 [36]	400	70	96	68
10%Ni/OMA(ordered mesoporous alumina) [36]	400	70	95	66
10%Ni3%Co/OMA(ordered mesoporous alumina) [36]	400	78	99	77
14%NiUSY [37]	400	25	61	15
CeNiUSY [38]	400	55	86	47

Despite their high activity, Ni catalysts are very sensitive to coke deposition or metal sintering because of high temperature reaction. An interesting solution to catalyst deactivation, that has been widely studied in the last years, is the addition of a second metal. Among these additional metals, Co was found to be interesting, because it has shown to improve the metallic Ni

dispersion and to increase the catalyst stability and resistance to deactivation [39–41]. Moreover, the price of cobalt is relatively lower than other metals used as second metal in methanation catalysts such as noble metals and cerium.

CO_2 methanation still needs to be improved in terms of process efficiency, reactor design and catalyst design. Therefore, our main objective is to contribute to the catalyst design improvement through the development of an efficient Ni or Ni-Co based catalyst with high stability and resistance to deactivation for further utilization in the industrial application. The use of the efficient catalysts, prepared in this work, will allow performing the CO_2 methanation reaction at relatively low temperatures and lowering the overall process energy consumption.

In this work, efficient Ni and Ni-Co supported alumina catalysts were prepared. Ni content was varied from 5 to 25% wt. and Co from 3 to 10% wt. The catalysts were characterized and tested in a CO_2 methanation reactor under atmospheric pressure. The optimized Ni-Co formulation was given. Finally, the remarkable stability of the efficient Ni based catalysts was proven through CO_2 methanation catalytic long duration tests (over 200 h).

2 Experimental

2.1 Catalysts preparation and characterization

Ni/Al_2O_3 and $Ni\text{-}Co/Al_2O_3$ catalysts were prepared by an original method developed by Azzolina-Jury [42]. The first step is the preparation of alumina extrudates. γ-alumina was prepared by calcination of boehmite powders (Sasol DISPAL 23N4-80) at 600°C for 4 h. Then a binder was added to alumina and the extrusion of the mixture was performed. The extrudates were calcined at 600°C for 4 h. Alumina extrudates of 3 mm diameter and 5 mm length were

impregnated with an aqueous solution of $Ni(NO_3)_2 \cdot 6H_2O$ (Acros Organics), or co-impregnated with both $Ni(NO_3)_2 \cdot 6H_2O$ and $Co(NO_3)_2 \cdot 6H_2O$ (Acros Organics) at 80 °C under partial vacuum. Catalyst samples were calcined for 4 h at 450 °C. Table 3 lists the prepared catalysts with their metal loading.

Table 3: List of Ni and Ni-Co catalysts

Catalyst	Ni (% wt.)	Co (% wt.)
5Ni	5%	0%
10Ni	10%	0%
15Ni	15%	0%
20Ni	20%	0%
25Ni	25%	0%
15Co	0%	15%
10Ni,10Co	10%	10%
15Ni,5Co	15%	5%
20Ni,3Co	20%	3%
20Ni,5Co	20%	5%
20Ni,8Co	20%	8%
20Ni,10Co	20%	10%

The surface area and porosity of the catalysts were estimated by nitrogen adsorption in a N_2 sorption analyser (Micromeritics ASAP 2020) at -196 °C. Before adsorption, samples were outgassed at 200 °C. X-ray diffraction (XRD) was performed using PANalytical X'Pert Pro diffractometer, equipped with a Cu-Kα radiation source to examine the crystallinity of the catalysts and to estimate the metal particle size. Temperature programmed reduction (H_2-TPR) was carried out in Micromeritics AutoChem II, equipped with a thermal conductivity detector (TCD), for evaluating the reducibility of the catalysts and for identifying Ni and Co states. TPR was performed under flow of 5% v/v H_2 in Ar from room temperature to 1000 °C. FTIR (Fourier

154 Transformation Infra-Red) measurements were performed using a Nicolet FTIR spectrometer.
155 Catalyst powders were pressed into self-supported wafers (15-20 mg) and placed inside the IR
156 cell under partial vacuum (10^{-6} Torr). Wafers were activated at 400 °C for 4 h and then reduced
157 twice under 100 Torr H_2 for 30 minutes. Two molecule probes were used: CO and pyridine. The
158 adsorption of CO on the wafer surfaces was carried out at room temperature, while the adsorption
159 of pyridine was performed at 150 °C to guarantee a good diffusion of the molecule. CO
160 adsorption provided information about Ni dispersion on the support surface. Several CO-metal
161 species can be formed from the interaction between CO and the metal (Ni or Ni-Co), which are
162 used to identify whether the metal is highly, moderately or poorly dispersed. The adsorption of
163 pyridine was used to evaluate the acidity (Lewis in this case) of the catalysts. All characterization
164 results will be developed and discussed in detail in a forthcoming paper. However, the useful
165 results for the catalytic activity interpretation are presented in Section 3.

166 Prior to the catalytic tests, all catalysts were sieved (1000 µm–1400 µm). An analysis by laser
167 granulometry (Malvern Mastersizer 3000) was carried out on five of our catalysts to precisely
168 measure the mean diameter of the particles. For each catalyst, the measurement was repeated for
169 five times, and the volume mean diameter D[4,3] (Brouckere Mean Diameter) [43] is presented in
170 Table 4. The values confirm that all the tested catalysts have a similar diameter around 1350 µm.

171
172

Table 4 : Volume mean diameter

Catalyst	D (µm)	Standard deviation (µm)
10Ni	1152	72
20Ni	1302	127
10Ni,10Co	1332	46
15Ni,5Co	1434	46

20Ni,8Co	1404	107

2.2 CO_2 methanation set-up

2.2.1 Experimental set-up

The methanation catalytic tests were performed under atmospheric pressure using the laboratory scale set-up shown in Figure ***1***. The reactor consists of a tubular stainless steel tube of 4 mm of inner diameter and 20 mm length. It was filled with 0.92 g of catalyst. Glass wool was introduced on both sides of the catalytic bed to ensure good gas dispersion and to maintain the catalytic bed at the centre of the tube. This reactor was inserted in a tubular furnace (Eraly). A K-type thermocouple T1 was inserted at the centre of the catalyst bed to measure the temperature during the reduction and methanation reaction. A second thermocouple T2, placed at the wall of the furnace, was used to regulate its temperature.

CO_2, N_2, and H_2 bottles were provided by Linde. The reactants' flow rates were controlled by three mass flowmeters. Gas mixtures were introduced into the reactor through a "mixer" consisting of a bed of inert particles. At the reactor outlet, a cold trap made from water ice (0 °C) allowed to remove the main part of water vapour from the outgoing gas stream. The by-pass between V4 and V5 was used for GC calibration. During methanation runs, V4 was closed, V5 was open, and the feed gas went through the reactor. The outgoing mass flowrate was then measured by a Coriolis flowmeter (Bronkhorst ML120). Piezoresistive pressure transducers (Keller PR-23 and Corame PTX-5072) were used to measure the operating pressure at two different places of the process.

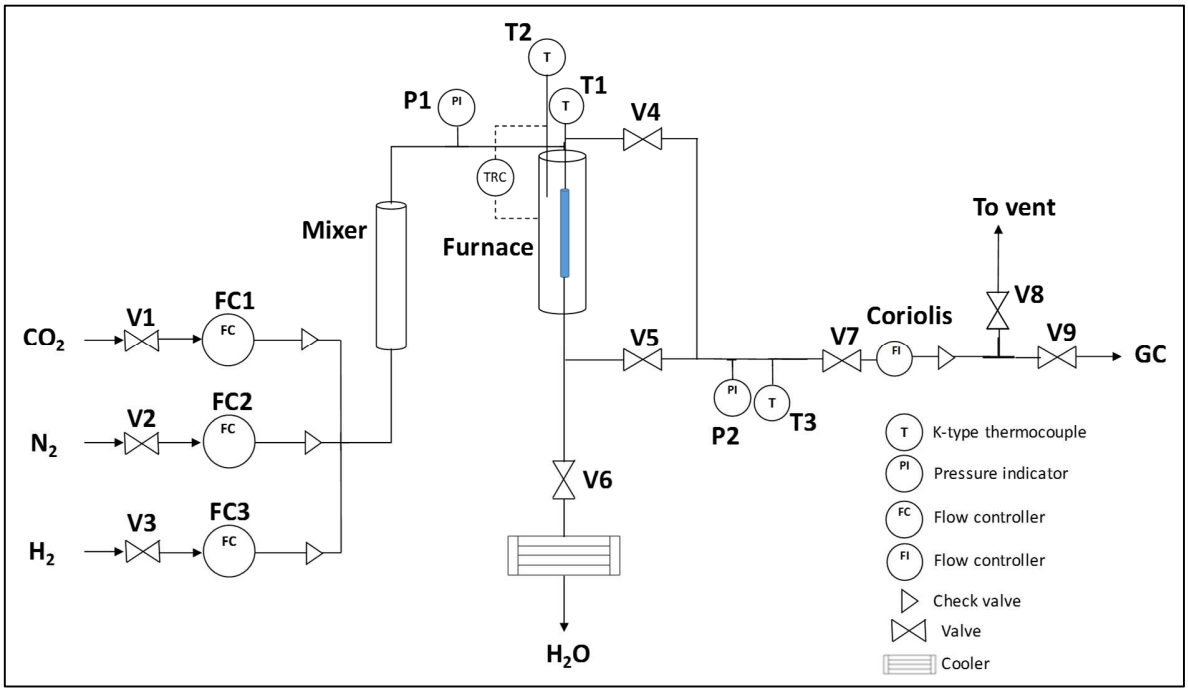

Figure 1: CO_2 methanation set-up at the atmospheric pressure

The outgoing gas was analysed using an on-line gas chromatograph from Perkin Elmer (Clarus 590). It is equipped with three columns, a methanizer and two detectors. Two Hayesep columns were used to separate CO_2, H_2/N_2, CO and CH_4, and a MolSieve column was used to quantify H_2 and N_2. TCD was used to measure H_2 and N_2 concentrations and Flame ionization detector (FID) was used to quantify CO_2, CO and CH_4 concentrations. FID detector was equipped with a methanizer consisting of a bed of catalyst that reduces CO and CO_2 to methane, which can be further detected by FID detector. TCD and FID temperatures were maintained at 150 °C and 400 °C, respectively. The calibration of peak areas was done using already known gas compositions. Coriolis flowmeter gives an accurate value of mass flow rate of the outgoing gas and coupled to the results of the GC, it leads to the composition of the output gas. CO_2 or H_2 conversion,

methane selectivity from H_2 or CO_2 conversion and methane yield from H_2 or CO_2 conversion were estimated using Equations (3)–(5):

$$X_i = 100 \times \frac{\dot{n}_i^0 - \dot{n}_i}{\dot{n}_i^0}, \quad (3)$$

$$S_{CH_4} = 100 \times \frac{\dot{n}_{CH_4}}{\dot{n}_i^0 \times X_{CO_2}} \text{ or } S_{CH_4} = 100 \times 4 \times \frac{\dot{n}_{CH_4}}{\dot{n}_i^0 \times X_{H_2}}, \quad (4)$$

$$Y_{CH_4} = 100 \times \frac{\dot{n}_{CH_4}}{\dot{n}_{CO_2}^0} \text{ or } Y_{CH_4} = 100 \times 4 \times \frac{\dot{n}_{CH_4}}{\dot{n}_{H_2}^0}, \quad (5)$$

where i CO_2 or H_2; $\dot{n}_i$ and $\dot{n}_i^0$ are the molar flowrate of i at the outlet and at inlet of the reactor respectively.

The catalytic activity and stability of the catalyst were evaluated by following CO_2 and H_2 conversion. The methane selectivity and yield were calculated with respect to CO_2 or H_2, according to Equations (4) and (5). The overall material balance was checked for each analysis. It was within ± 5% mol. It was noticed that no other product was detected and that CO_2 and H_2 conversions were identical, within experimental error ± 5%.

2.2.2 Experimental procedure and operating conditions

For each experiment, 0.92 g of sieved catalyst particles (1350 µm of mean diameter) was loaded into the reactor and then the reactor was vibrated, packed and assembled. The height of catalyst bed was measured and it was 10 cm for all experiments. A leak test was accomplished to ensure the sealing of the set-up and to avoid any hydrogen leak. Then, the catalyst was reduced under a continuous flow of 5% v/v H_2 in N_2 at the total flow rate of 200 mL/min STP (Standard

227 Temperature and Pressure conditions) and at 400 °C under atmospheric pressure. The
228 composition of the inlet gas mixture was first estimated by gas chromatography (GC) analysis
229 using the bypass before being introduced into the reactor. The methanation reaction was
230 conducted at several temperatures under atmospheric pressure. For each temperature, GC
231 analyses were conducted every ten minutes until steady state was well established. Thereon, three
232 samples were taken each 10 minutes, analysed and the mean values calculated as results. After
233 the analysis, the temperature of the furnace was adjusted to the next value to obtain a new
234 operating point. The temperature was increased from 100 °C to 400 °C, followed by a decrease
235 from 400 °C to 100 °C to detect the possible hysteresis phenomena. The feed gas mixture
236 containing CO_2 and H_2 was passed continuously through the catalyst bed with a total flow rate of
237 200 mL/min STP and a molar composition CO_2:H_2:N_2 = 1:4:5. The CO_2:H_2 ratio = 1:4 has been
238 chosen considering the results of Goa et al.(2012)[44], and Sahebdelfar et al.(2015)[45] who
239 found that a ratio equal to 1:4 is the optimum for CO_2 conversion and methane selectivity and that
240 a ratio equal or lower than ¼ avoids carbon deposition [44]. The feed has been diluted with N_2 to
241 ensure good hydrodynamic conditions in the catalytic bed such as a non-laminar flow and a
242 sufficiently efficient external transfer and by the time, to avoid an excessive temperature increase
243 in the catalytic bed due to the exothermicity of the reaction.

244 # 3 Results and discussion
245

246 ## *3.1 Preliminary results and discussions*
247

248 Concerning the CO_2 methanation, some preliminary results are worthwhile to be given:

a) No conversion (CO_2 or H_2) has been observed below 150 °C, irrespective of the catalyst being used. The reaction is not occurring. Catalytic results are then presented from 150°C.

b) Figure 2 shows the typical results for any Ni or Ni-Co catalyst.

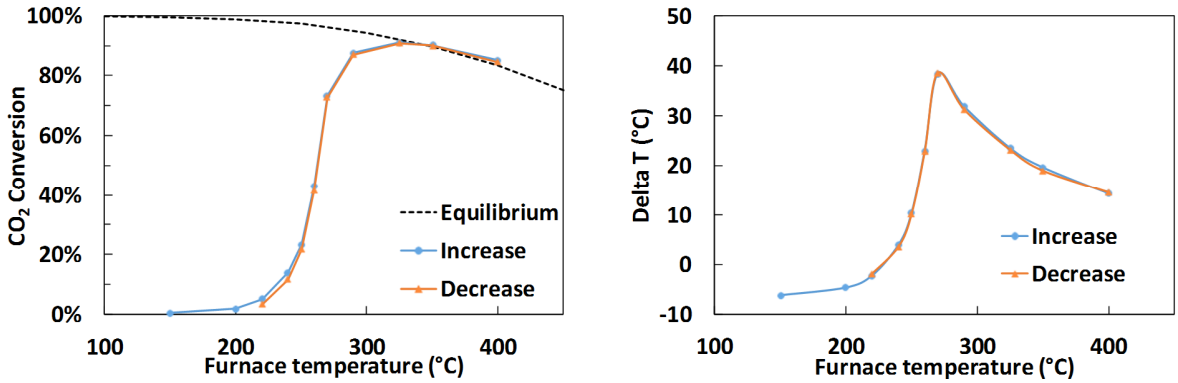

Figure 2: Hysteresis test on methanation results for 20Ni catalyst

In Figure 2a, conversion is reported for a 20% wt. Ni catalyst and the thermodynamic equilibrium of the reaction, which was obtained by simulation using Aspen Plus. The reaction starts around 200 °C and hydrogen (or CO_2) conversion increases with the increase in the furnace temperature and the reaction temperature. The shape of the conversion curve indicates a sharp acceleration of the reaction rate around 250 °C, which corresponds to the transition from the extinct state to a lighted state of the bed. When the bed is extinct, methanation occurs progressively all along the catalytic bed; but when the bed is lighted, the main part of the reaction occurs in a small zone of the catalytic bed, where the temperature is much higher than the furnace one (+40°C), because of the reaction exothermicity. This state leads to high conversions (around 80-90%). When the furnace temperature is increased above 350 °C, the CO_2 conversion decreases (Figure 2a) because of the thermodynamic equilibrium limitation (dotted line). The difference of temperature between the centre of the bed and the furnace temperature, called DeltaT, is presented in Figure 2b. A

maximum of DeltaT can be observed when the furnace temperature approaches 280 °C. The shape of this curve clearly indicates that, for each steady state, the temperature is not homogeneous all along the catalytic bed and a temperature gradient is verified. The temperature all along the bed passes by a maximum value, but the position of this value depends on the operating conditions. The position of this peak is directly linked to the activity of the catalyst. The more active it is, the highest this peak is and positioned close to the inlet of the bed. That is the reason why the DeltaT curve, measured at the centre of the bed, also passes through a maximum when increasing the furnace temperature. It is also important to note that the measured DeltaT does not obviously include the real maximum. In fact, this curve is always very sharp and the real maximum value is probably missed, but it gives an order of magnitude.

c) Because hysteresis is an indication of the existence of multiple steady states and has already been reported in fixed bed reactors for similar reactions [46,47], we first investigated this phenomenon in our system. As shown in Figure 2, no hysteresis was observed when conducting the experiments with an increasing or a decreasing temperature. The conversions and the DeltaT curves were rigorously the same. These curves also prove the good reproducibility of the experiments and whether any deactivation occurs, at least after one run going back and forth.

d) The GC analysis detects by-products that can be formed during the methanation, such as CO, and C1-C4 hydrocarbons. For all of our GC measurements made, while studying and comparing methanation products for different Ni and Ni-Co catalysts, no C1-C4 hydrocarbon by-products were detected. Only methane was detected and then quantified. CO was detected but in extremely low quantities (<1/1000)—smaller than the standard deviation of the method. Hence, the selectivity of CH_4 is 100% with all catalysts, and its yield is equal to the conversion of CO_2 or H_2.

3.2 *Effect of Ni loading on catalytic activity and selectivity*

The catalytic activity as a function of furnace temperature of various Ni/Al_2O_3 catalysts with Ni content varying from 5 to 25% wt. is shown in Figure 3.

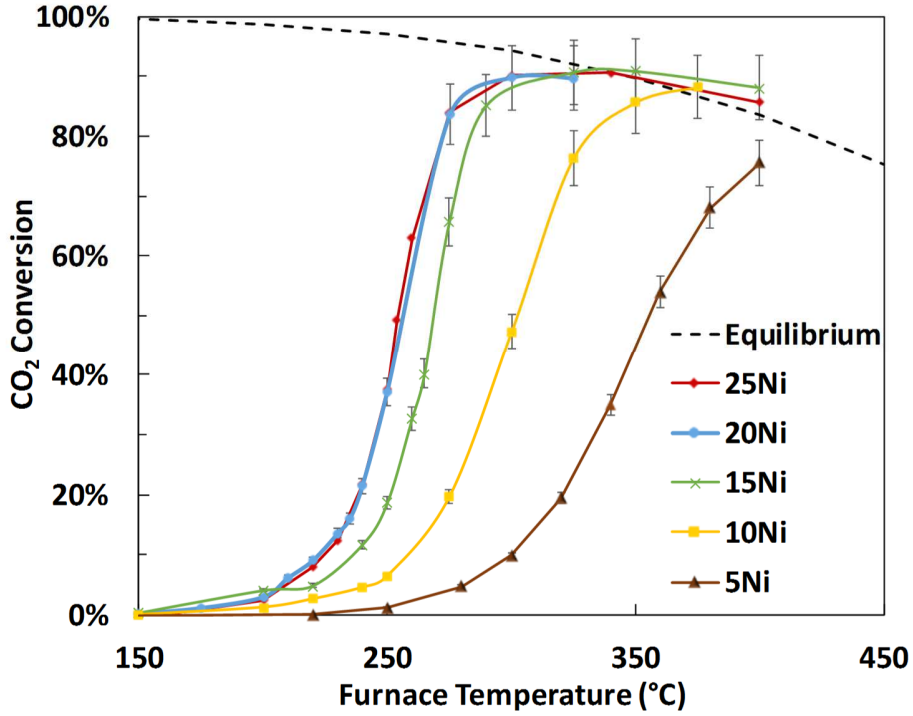

Figure 3: Effect of Ni content on H_2 conversion. Gas Hourly Space Velocity (GHSV) = 9554 h^{-1} (=13043 mL STP/g_{cat} h), H_2/CO_2=4/1

CO_2 conversion increases with temperature for all catalysts. The temperature ignition of the reactor is observed to happen between 200 and 250 °C. At this temperature, the conversion dramatically increases to reach a maximum of about 90% for all the catalysts, with Ni content higher than 5%. Afterwards, the conversion starts decreasing with increasing temperature. As explained above, the reaction takes place essentially on a limited zone of the catalyst bed and the

rest of the bed is used to establish the equilibrium. This is proved by the superposition of conversion curves on the equilibrium curve at the highest temperature for all the catalysts. For the high temperatures of the furnace, the thermodynamic equilibrium is reached at the outlet of the reactor. It is known that the methanation reaction is accompanied with CO production via reverse water-gas shift reaction (Equation 2). The methanation of CO can then occur, according to the following the reaction (Equation 6):

$$CO + 3H_2 \longleftrightarrow CH_4 + H_2O \qquad \Delta H_{298\,K} = -206.1\ kJ/mol,\ \Delta G^0 = -141.8\ kJ/mol \qquad (6)$$

The produced CO, formed in the first part of the catalytic bed, is converted in the rest of the bed into methane, and this is why the selectivity of methane is always 100%.

The catalytic activity increases with Ni loading between 5 and 20% wt., as expected (Figure 3). The more Ni is incorporated, the more catalytic sites are usually available for the reaction. Nevertheless, the catalyst with 25 % wt. Ni loading shows an activity very similar to that of the catalyst with 20% wt. Ni. This indicates that there is no benefit in using a Ni catalyst with higher Ni loading than 20%. This trend can easily be explained by our characterization results presented in Table 5, that summarizes the textural properties of our Ni catalysts and their percentage of reduced Ni.

Table 5: The properties of Ni catalysts

Catalyst	BET surface area (m^2/g)	Pore volume[a] (cm^3/g)	Crystallite size[b] (nm)	Reduced Ni at 500 °C[c] (%)
5Ni	166	0.40	nd	nd
10Ni	153	0.36	6	1.8
15Ni	144	0.32	8	2.0
20Ni	141	0.30	10	6.2
25Ni	141	0.29	10	4.4

[a] BJH desorption pore volume.

[b] NiO (220) crystallite diameter calculated using Scherrer equation [48] from X-ray diffraction (XRD) patterns.

[c] percentage of reduced Ni at 500 °C calculated from TPR profiles.
nd = non detectable

The X-ray diffraction (XRD) analysis confirmed the presence of Ni on γ-alumina. The peaks of Ni were identified and they became, as expected, sharper as the metal loading increased. The surface areas were estimated between 166 and 140 m^2/g and decreased when increasing the Ni content. For instance, a decrease in the surface area of 15% was observed, when the Ni amount was varied from 5% to 25% wt. The porous volume was also affected and decreased by 25%, from 0.4 cm^3/g to 0.3 cm^3/g. This fact can be explained by the increase of the Ni amount within alumina pores [28,49]. The average size of NiO particles were estimated using the Scherrer equation. NiO particle size increases with Ni loading from 6 to 10 nm. For 5 % wt. Ni, NiO particle size cannot be estimated, because NiO is highly dispersed and is not detectable by XRD analysis. Ni active particles are more available with the increasing Ni content, but they are less dispersed over the support. Thus, Ni particle size is increased. This fact is verified through FTIR CO adsorption. Table 6 presents the percentage of moderately and highly dispersed Ni on prepared Ni catalysts, calculated from FTIR CO adsorption characterization. This percentage decreases from 43.8% to 37.7%, when increasing Ni loading from 5% to 25%. These results correspond to the sum of the two adsorption states of CO [50] on reduced Ni, in the region between 2030 and 2070 cm^{-1}. Both adsorption states are linear—the first corresponds to mono-carbonyls and the second to multi-carbonyls. The results of CO adsorption are consistent with those reported in the literature [28] and prove that the Ni dispersion decreases with its increased loading.

Table 6: Ni dispersion by FTIR CO adsorption

Moderately and Highly dispersed Ni

Configurations / Catalysts	CO Ni	CO CO Ni
5Ni	43.8%	
10Ni	41.4%	
15Ni	36.9%	
20Ni	34.3%	
25Ni	37.7%	

Concerning the reducibility of the species, the percentages of reduced Ni at 500 °C, given in Table 5, were calculated from H_2-TPR profiles. It increases up to 6.2% for 20% wt. Ni, then decreases to 4.4% for 25% wt. Ni catalyst. This shows that the reducibility of Ni catalyst increases with the Ni loading from 5% wt. Ni to 20% wt. Ni, but decreases hereafter. In fact, the species that may be present on the surface of the prepared catalysts are NiO and $NiAl_2O_4$. To reduce $NiAl_2O_4$ species, a very high temperature (over 800 °C) is required, while the reduction of oxides usually begins at 300 °C. NiO may either be weakly or strongly bonded to the support. For example, if the particles are hemispherical, 25% of the NiO phase will be in contact with the alumina support surface. Such intimate contact between the two phases would result in a strong interaction and the NiO species' reducibility could be difficult [51]. Indeed, a relation between the results of particle size to those of TPR could be established in this way. The increase in the NiO particle size, between 5Ni and 20Ni (Table 5), results in the formation of weakly bonded NiO to alumina support, and thus the reducibility of the catalysts is increased.

DeltaT for several Ni catalysts is presented in Figure 4.

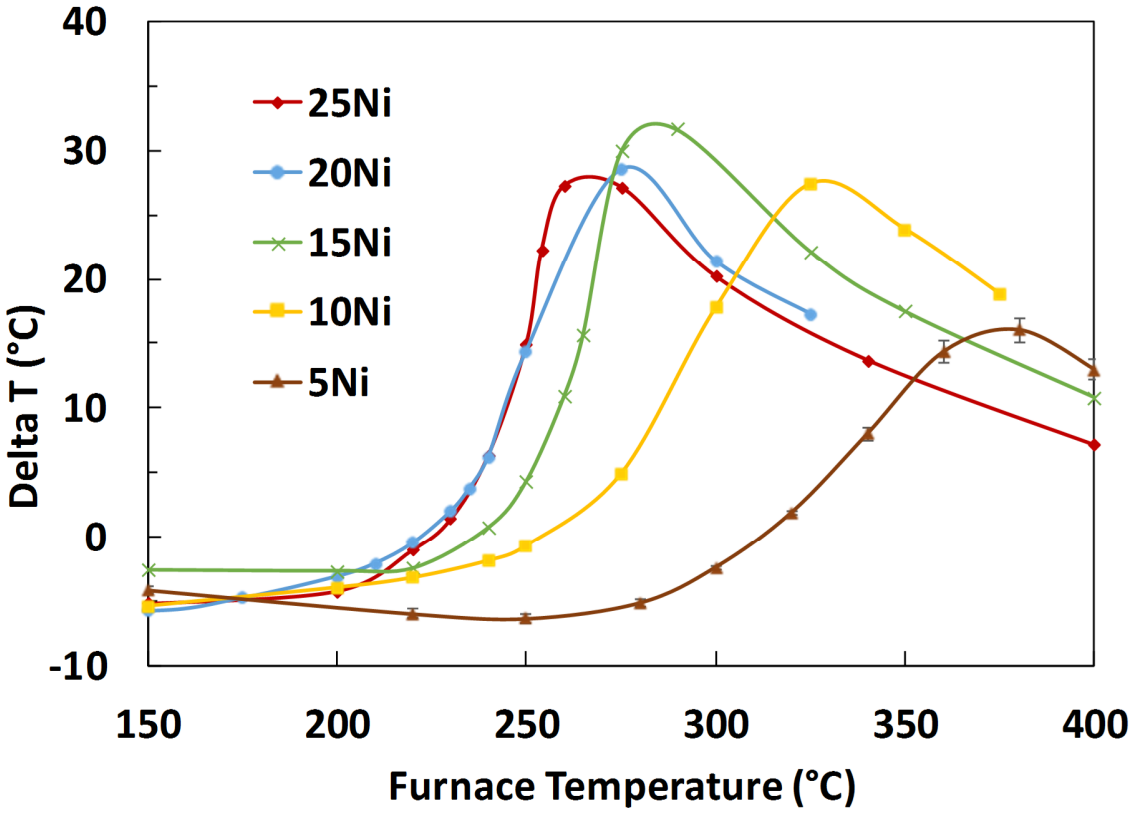

Figure 4: Temperature increase from the inlet to the centre of the bed for several Ni contents

DeltaT curves show evidence of the exothermicity of the methanation reaction. Because of the thermal resistances, when the reaction does not occur or is very slow, DeltaT can be negative; but it reaches a maximum of 34 °C with the 15Ni catalyst, when the regulated furnace temperature is 290 °C. The catalysts with 20% wt. and 25% wt. Ni show similar DeltaT profiles, in accordance with their similar activity. 5Ni and 10Ni catalysts have lower delta T values. The furnace temperature, for which DeltaT is maximum, is not the same for all the catalysts; and the more the catalyst is active, the lower the temperature is. So, this maximum value shifts to the right, towards high furnace temperatures, as the Ni content decreases. This means that with less Ni, it is necessary to raise the temperature of the oven to carry out the methanation reaction and to obtain

375 a significant conversion of CO_2. The maximum values, showed in Figure 4, do not necessarily fit
376 the maximum temperature in the whole bed. The highest temperature is reached in the narrow
377 zone, where most of the reactions take place. This hot zone becomes larger when the catalyst is
378 less loaded with Ni. When the temperature of the furnace is increased, the conversion peak, and
379 therefore the hot zone are moved towards the reactor inlet. The K-type thermocouple, placed at
380 the centre of the bed, will detect the increase and decrease in temperatures, because it will be
381 crossed by the hot zone during the variation in the furnace temperature.

382 Finally, increasing the Ni content in the catalysts offers numerous and reducible active sites, that
383 are less dispersed and accessible. The global activity of the catalysts, showed in Figure 3, is the
384 result of all these combined effects showing that 20% is close to the optimum value for Ni
385 content. The exothermicity is moderate in our conditions and the maximum value of DeltaT (and
386 its position on Figure 4) is an indication of the catalysts' activity.

387 *3.3 Effect of Co content on CO_2 conversion*
388

389 The effect of Co addition on methanation reaction was investigated based on H_2 and CO_2
390 conversion and CH_4 selectivity. The synthetized catalysts of Table 3 were tested in the CO_2
391 methanation pilot at several reaction temperatures under atmospheric pressure with a molar ratio
392 $H_2/CO_2 = 4/1$.

393 The catalytic effect of Co on CO_2 methanation was firstly evaluated by performing a test with a
394 catalyst containing Co only (15Co), supported on gamma-alumina. In Figure 5, the results are
395 compared with those obtained with 15Ni and with a third catalyst containing 15% wt. Ni, 5% wt.
396 Co (15Ni,5Co).

397

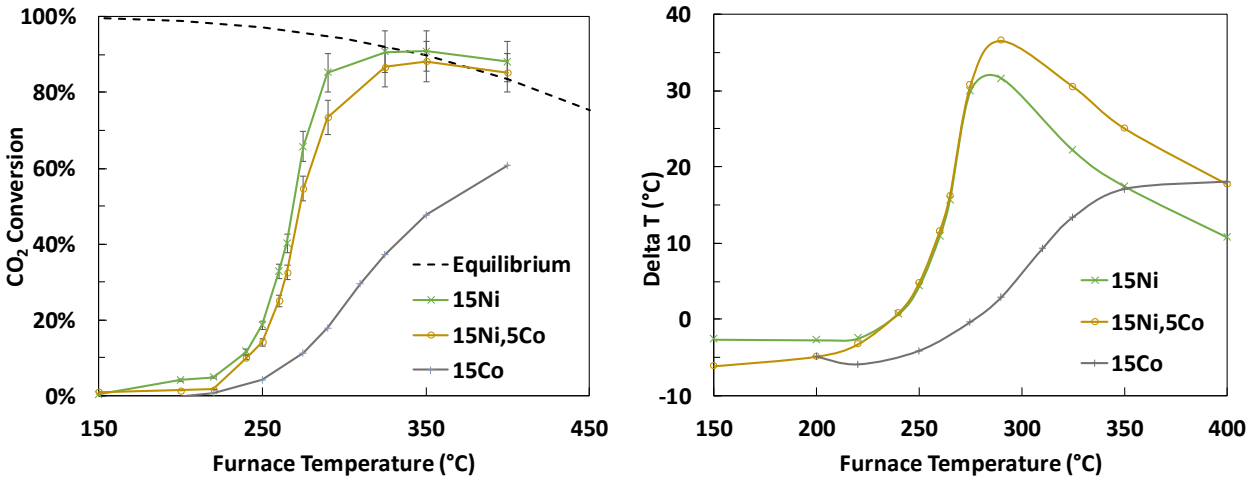

Figure 5: CO_2 conversion and DeltaT for 15Co, 15Ni and 15Ni, 5Co catalysts

It was found that Co is an active catalyst for CO_2 methanation reaction, because CO_2 and H_2 are partially converted into methane. The methane selectivity was found to be 100%, when Co alone was used as in the case of 15Ni (Ni alone). Co was less active than Ni. No catalytic activity enhancement was observed while using a catalyst containing 15Ni, 5Co.

Figure 6a shows CO_2 conversion for 20% wt. Ni catalysts, with and without Co. The conversion for all the five catalysts is nearly the same and no differences in the catalysts' activity were observed. DeltaT curves (Figure 6b) are also very similar for 20Ni without Co, and with 3%, 5%, 8% and 10% Co indicate that adding Co to a 20Ni catalyst is not worthwhile in terms of activity. Otherwise, the catalyst with 10Ni, 10Co behaves differently and shows a higher activity than the one containing 10% wt. Ni at low temperature (Figure 4c and 4d). At 300 °C, conversion with 10Ni catalyst is around 47%, but is increased to 75% when adding 10% Co to the catalyst. DeltaT

maximum is also shifted towards the lower furnace temperatures. This indicates that for low Ni content, Co addition improves the conversion, but that is not the case with higher Ni loadings. The catalyst 10Ni,10Co offers good performances allowing less Ni usage and obtaining slightly lower conversion than 20Ni, which is still an interesting finding.

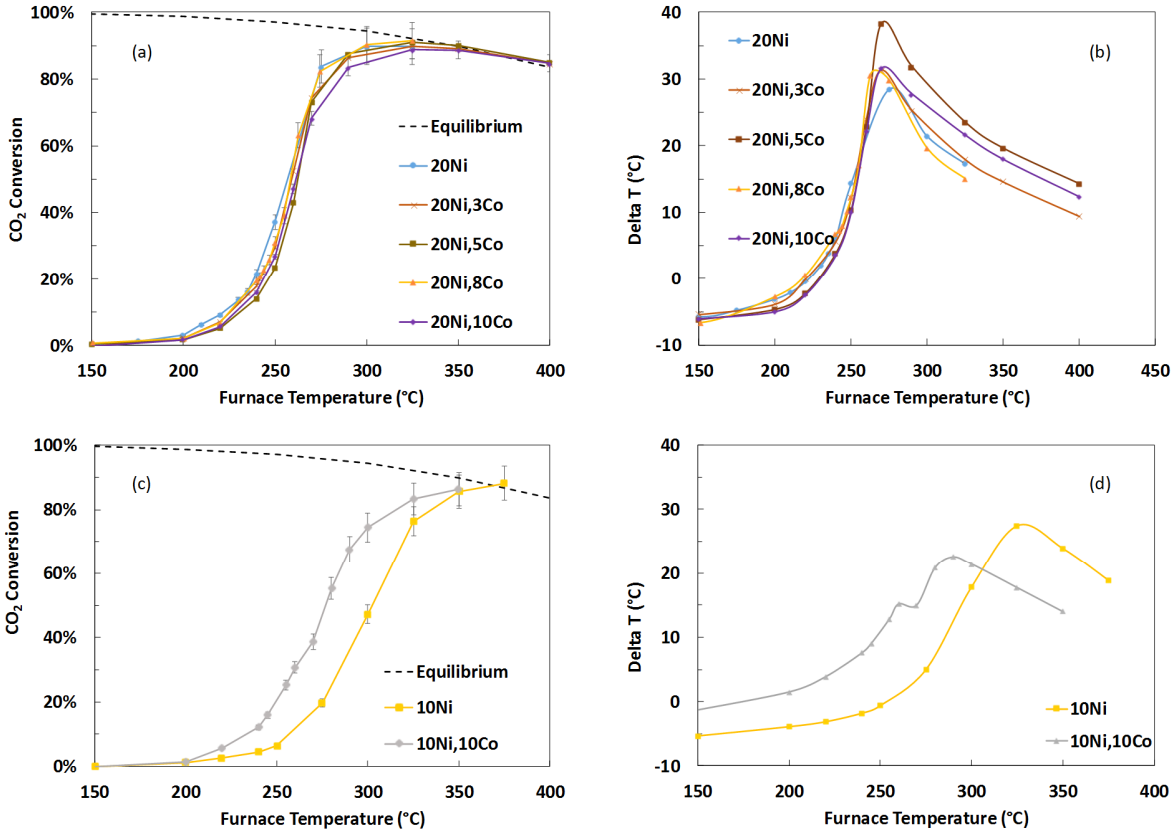

Figure 6: CO_2 conversion (a,c) and DeltaT (b, d) for methanation with Ni-Co catalysts of various contents

The main characterization results of Ni-Co are summarized in Table 7.

Table 7: Ni- Co catalysts characterization

Catalyst	BET surface area (m^2/g)	Pore volume [a] (cm^3/g)	Reduced Ni/Co at 500 °C [b] (%)	Adsorbed CO (µmol/g)

20Ni	140	0.30	6	71.5
20Ni,5Co	134	0.30	13	63.1
20Ni,10Co	132	0.28	28	52.2
15Ni	144	0.32	2	66.6
15Ni,5Co	143	0.32	nm	145
10Ni	153	0.36	2	49.9
10Ni,10 Co	141	0.32	31	48.5
15Co	137	0.32	23	9.5

427 [a] BJH desorption pore volume.
428 [b] percentage of reduced Ni/Co at 500 °C calculated from TPR profiles.
429 nm = not measured
430

431 BET surface and pore volume are not much affected by Co addition, despite the fact that it
432 overcharges this catalyst with metals. But the percentage of reduced species at 500 °C is strongly
433 increased when Co is added as shown for 20%Ni-Co and 10%Ni-Co catalysts. Thus, Co addition
434 increases the reducibility of the Ni catalyst, which has a positive effect on activity. The CO
435 adsorption of catalysts is also influenced by Co addition. For high Ni content (20%wt.), the
436 adsorbed CO decreases with the Co content. Ni dispersion is not favoured by the Co introduction,
437 because the total amount of metal (Co + Ni) is high. However, for intermediate Ni content (15%
438 wt.), Ni dispersion was remarkably improved by Co introduction. No differences in terms of Ni
439 dispersion were observed after lowering the Ni content (10% wt.) and increasing the Co amount
440 (10% wt.). The Co introduction improves Ni reducibility in all cases. Nevertheless, the Co
441 introduction favours Ni dispersion, when the catalyst is not overcharged with both metals. For
442 high Ni loaded catalysts, the benefits of Co addition, through a better reducibility, are
443 counterbalanced by the overcharge of the catalyst and a worse dispersion of the active species.
444 These results are in good agreement with the recent studies of Liu et al. [36] and Xu et al. [52],
445 who also found a promotion effect of Co on Ni catalysts.

446

3.4 Deactivation-Stability

The stability of the catalysts is a very important point that has to be examined when designing new catalytic processes. Considering the above results, it was decided to perform long catalytic methanation tests over 200 h with 0.09 g of 10Ni, 10Ni,10Co, and 20Ni catalysts at 350 °C. The catalysts were first reduced under a continuous flow of 5% v/v H_2 in N_2 at the total flow rate of 200 mL/min STP and at 400 °C under atmospheric pressure. Relatively low reaction temperature (350 °C) was chosen, because it already allowed a very high conversion of CO_2 into methane (85% for 10Ni catalyst in Figure 6c) for 0.92 g of catalyst, despite choosing the low temperature. We also decided to divide the catalyst weight by 10 to run it with high methanation rates all along the bed, which is now only one centimetre long. The objective was to limit the lifetime test and see whether deactivation occurs. Figure 7 shows CO_2 conversion and CH_4 and CO selectivity during the 200 h of reaction.

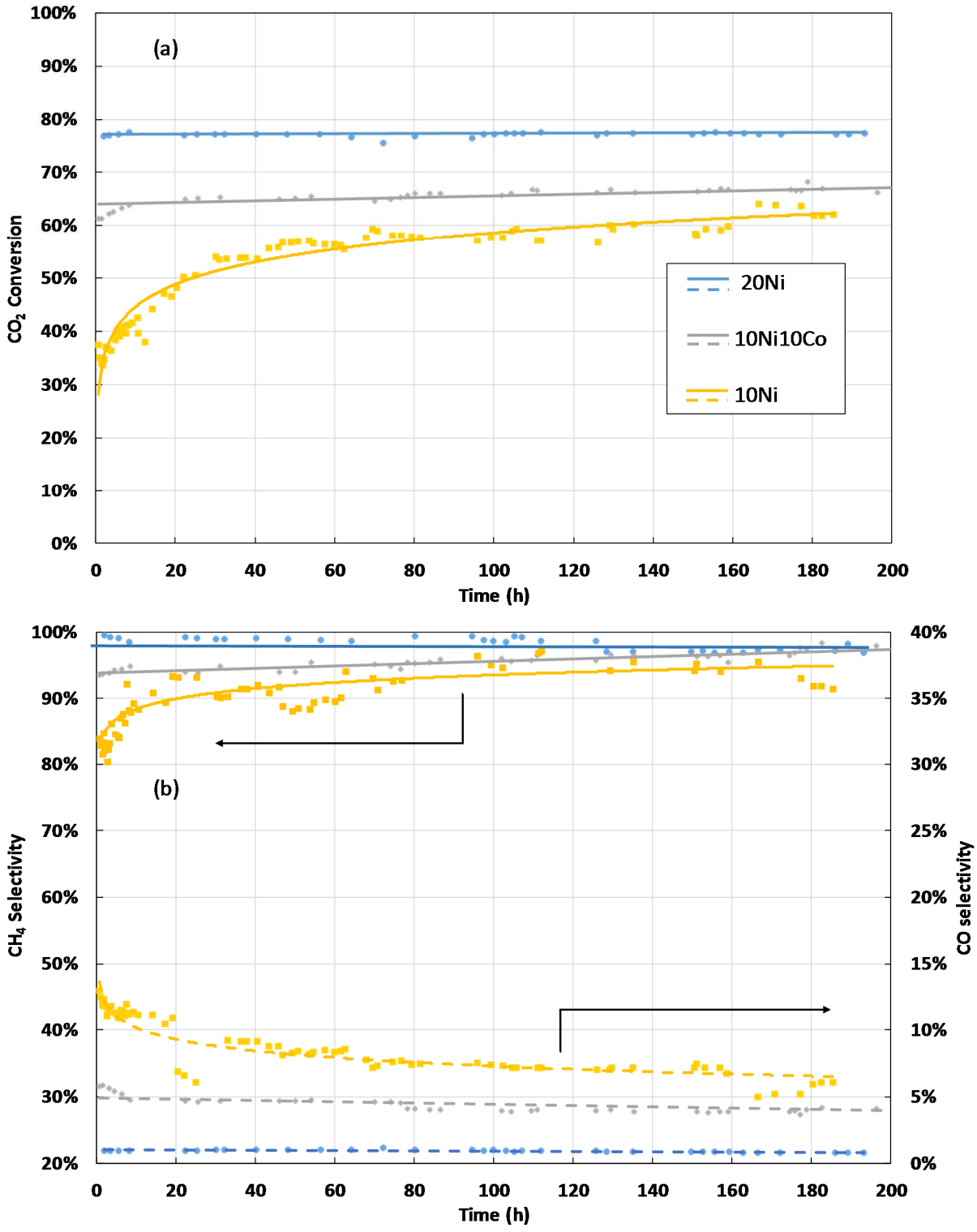

Figure 7.Stability test on 10Ni, 10Ni,10Co, and 20Ni catalysts: (a) CO_2 conversion, (b) CH_4 and CO selectivity (T= 350 °C, Catalyst mass= 0.09g)

As shown in Figure 7, the initial conversions obtained with 10Ni; 10Ni,10Co and 20Ni catalysts are 32%, 61.5% and 77% respectively. These conversions are observed with 0.09 g of catalyst only. CO is now detected and quantified so methane selectivity is not 100% anymore (Figure 7 (b)). CO is the only by-product that is detected using the three catalysts. In this configuration, the catalytic bed is not long enough to fully convert CO_2 and transform CO in methane, according to Equation (6), but this configuration is very helpful to follow the course of the reaction with time. Figure 7 shows that 10Ni and 10Ni,10Co catalysts exhibit an activation phase, for which CO_2 conversion and methane selectivity keep on increasing, whereas CO selectivity decreases. The more active the catalyst is, the faster the activation phase is and this latter is even not visible for 20Ni catalyst. 20Ni catalyst maintains a CO_2 conversion of 77% and a CH_4 selectivity equal to 98% during all the 200 h of stability test. For 10Ni catalyst, during the first eighty hours, CO_2 conversion increases from 32% to 56% and then stabilizes. Methane selectivity also stabilizes at around 95%. During the following 120 h, the catalyst activity and selectivity are maintained and no deactivation is observed. For 10Ni,10Co catalyst, CO_2 conversion stabilizes at 67 % and CH_4 selectivity at 97% after 20 h of reaction until the end of the long-term test. The three tested catalysts show high stability during 200 h of reaction. This result is remarkable and, with the exception of Liu et al. (2012) [59] who reported the good stability of a 15%Ni on alumina catalyst doped with 2%CeO_2 over 120h, such long-term experiments without deactivation are rarely reported in the literature.

Concerning the activation phase, an additional reduction of the NiO particles probably occurs at the beginning of the run. The preliminary reduction of the catalyst, done before methanation, is perhaps not long enough to fully reduce all the NiO particles, especially the ones which are not

well dispersed. Due to the heat of reaction, the bed temperature reaches at least 390°C for the 10Ni catalyst. This value is comparable to the reduction's one of 400°C, leading to additional reduction.

The methane production rates in $mol.h^{-1}.gNi^{-1}$ have also been calculated for our 10Ni; 10Ni,10Co and 20Ni catalysts and are compared to the reported values from the literature (Table 8). Our 10Ni catalyst shows a high methane production rate, better than most of the other catalysts containing 10% wt of Ni and comparable to the 10% Ni/CeO_2 tested by Tada et al.[53]. Our Ni on alumina support gives comparable results to the one supported on CeO_2 with the main advantage of a lower price and availability. Our 20Ni catalyst also exhibits good performances; at 325 °C, methane production rate is only 2.71 times less than the one presented in Garbarino et al. [57]. However, these authors reported results obtained at 400 °C with a 5:1 H_2:CO_2 ratio, representing much favourable conditions for the reaction. The 10Ni,10Co catalyst also shows a higher efficiency than other Ni-Co catalysts reported in the literature, even higher than those. supported on ordered mesoporous Alumina [52] or doped with cerium [59] which is more expensive than cobalt. Finally, even some more active Ni catalysts can be found in the literature [54–56]. They all use more expensive supports than alumina—sometimes structured—that create additional costs to the process.

Table 8: Comparison of methane production rate for various Ni catalysts on alumina

Author	Catalyst	Methane production rate ($mol.h^{-1}.g\ Ni^{-1}$)	GSHV ($mL.g_{cat}^{-1}.h^{-1}$)	GSHV (h^{-1})	T (°C)	H_2/CO_2	m_{cata} (g)	X_{CO_2}	S_{CH_4}
10Ni (this study)	10%Ni/Al_2O_3	3.2	133000		350	4	0.09	56	95
Tada et al. [53]	10%Ni/CeO_2	3.32		10000	350	4	0.3	90	100
Zhou et al. [27]	10%Ni/CeO_2	0.9	22000		340	4.6	0.1	91.1	100
Xu et al. [52]	10%Ni/Al_2O_3-	0.85	15000		400	4	0.1	68	97.5

Rahmani et al. [28]	OMA 10%Ni/ Al_2O_3	0.58	9000		350	3.5	-	70	91
Le et al. [57]	10%Ni/ CeO_2	0.27	60000		220	50	0.1	100	100
Liu et al. [36]	10%Ni/ Al_2O_3	0.16	10000		350	4	0.1	25	94
20Ni (this study)	20%Ni/ Al_2O_3	2.2	120000		325	4	0.92	90	100
Garbarino et al.[58]	20%Ni/ Al_2O_3	5.97		55000	400	5	-	80	78
Zhou et al.[54]	6.17% Ni/TiO	24.27		60000	350	4	0.05	73.2	96
Aziz et al. [55]	2 5%Ni/ MSN	11.75	50000		300	4	0.2	64.1	99.9
Aldana et al.[56]	5%Ni/S iO_2	3.89	22000		400	4	0.15	35	88.3
10Ni,10Co **(this study)**	10%Ni/ Al_2O_3	3.25	133000		350	4	0.09	61.5	95
Xu et al.[52]	8%Ni2 %Co/ OMA	1.22	15000		400	4	0.1	80	97.5
Liu et al.[59]	15%Ni 2%CeO 2/Al_2O_3	0.71	10000		350	4	0.1	85	94
Liu et al.[36]	10%Ni 3%Co/ Al_2O_3	0.49	10000		350	4	0.1	78	99

505

506 Finally, it is obvious that a global costs balance including the metals and support prices and the
507 lifetime of the catalyst, as well as mass and energy balances and heat losses calculations would
508 lead to a more precise analysis. However, considering our results, the Ni and Ni-Co catalysts
509 prepared in this study are likely to represent an improvement for further developments of
510 methanation processes: they combine a very good efficiency with a remarkable stability at low
511 temperature of 350°C. Stability ensures savings on catalysts costs. High methane production rates
512 per gram of Ni are reached at a lower level of temperature than the classical one, which is
513 favourable to energy savings. Moreover, cobalt can be used to dope low content Ni catalysts

514 (10%wt Ni as an example): it improves the catalyst activity by improving Ni reducibility and
515 dispersion and its excellent stability has also been demonstrated.

516

517 # 4 Conclusion
518

519 Ni and Ni-Co/γ-Al_2O_3 catalysts with optimum amounts of Ni and Co toward methanation
520 were prepared and characterized by several techniques. They were tested for CO_2 methanation
521 under atmospheric pressure. The experimental results showed that these catalysts were very
522 active even at low temperature (300–350 °C) for the CO_2 and H_2 conversion. The selectivity in
523 CH_4 was 100% as long as the catalytic bed was long enough to allow CO methanation and
524 equilibrium at the outlet of the reactor. The conversion and CH_4 selectivity were strongly affected
525 by Ni metal content. The addition of Co improved the reducibility of Ni species and metal
526 dispersion. The positive effect of Co addition was only observed with catalysts having low Ni
527 loading (below 10% in weight). From our results, the Co doped catalyst (10Ni,10Co) is more
528 active than the 10Ni at low temperature. It could be operated at 300°C and give comparable CO_2
529 conversion and methane yields to 10Ni at 350°C, which from a process point of view, should
530 reduce the energy consumption. Long life-test experiments at 350 °C with the 10Ni; 10Ni,10Co
531 and 20Ni catalysts already showed a higher CO_2 hydrogenation rate and a higher methane
532 production rate when compared with other similar catalysts in literature and presented a
533 remarkably good stability over 200 h run. The very good stability of our novel catalysts tested
534 over 200 h, and their high activity compared to other catalysts in the literature make them good
535 candidates for developing greener methanation processes.

536

Acknowledgements

The authors gratefully thank the project GENCOMM-NWE334 for the financial support. The project GENCOMM has been funded by the European Union with the European Regional Development Fund (ERDF) through the Interreg North-West Europe Program.

References

[1] N.G.C. Change, Carbon dioxide concentration | NASA Global Climate Change, Climate Change: Vital Signs of the Planet. (n.d.). https://climate.nasa.gov/vital-signs/carbon-dioxide (accessed September 7, 2018).

[2] M. a. A. Aziz, A.A. Jalil, S. Triwahyono, A. Ahmad, CO_2 methanation over heterogeneous catalysts: recent progress and future prospects, Green Chem. 17 (2015) 2647–2663. doi:10.1039/C5GC00119F.

[3] W. Wang, S. Wang, X. Ma, J. Gong, Recent advances in catalytic hydrogenation of carbon dioxide, Chem. Soc. Rev. 40 (2011) 3703–3727. doi:10.1039/C1CS15008A.

[4] G.A. Meehl, W.M. Washington, W.D. Collins, J.M. Arblaster, A. Hu, L.E. Buja, W.G. Strand, H. Teng, How Much More Global Warming and Sea Level Rise?, Science. 307 (2005) 1769–1772. doi:10.1126/science.1106663.

[5] A. Zervos, C. Lins, L. Tesnière, Mapping Renewable Energy Pathways towards 2020 - EU Roadmap, Brussels, Belgium, (2011). https://refman.energytransitionmodel.com/publications/1761 (accessed September 7, 2018).

[6] J. Ducamp, A. Bengaouer, P. Baurens, I. Fechete, P. Turek, F. Garin, Statu quo sur la méthanation du dioxyde de carbone : une revue de la littérature, Comptes Rendus Chimie. (2017). doi:10.1016/j.crci.2017.07.005.

[7] M. Sarić, J.W. Dijkstra, W.G. Haije, Economic perspectives of Power-to-Gas technologies in bio-methane production, Journal of CO_2 Utilization. 20 (2017) 81–90. doi:10.1016/j.jcou.2017.05.007.

[8] S. Rönsch, J. Schneider, S. Matthischke, M. Schlüter, M. Götz, J. Lefebvre, P. Prabhakaran, S. Bajohr, Review on methanation – From fundamentals to current projects, Fuel. 166 (2016) 276–296. doi:10.1016/j.fuel.2015.10.111.

[9] P. Sabatier, J.B. Senderens, C. R. Acad Sci Paris 134 (1902) 514-516, (n.d.).

566 [10] J. Kopyscinski, T.J. Schildhauer, S.M.A. Biollaz, Production of synthetic natural gas (SNG) from
567 coal and dry biomass – A technology review from 1950 to 2009, Fuel. 89 (2010) 1763–1783.
568 doi:10.1016/j.fuel.2010.01.027.

569 [11] T. Schaaf, J. Grünig, M.R. Schuster, T. Rothenfluh, A. Orth, Methanation of CO_2 - storage of
570 renewable energy in a gas distribution system, Energy, Sustainability and Society. 4 (2014) 2.
571 doi:10.1186/s13705-014-0029-1.

572 [12] Audi e-gas Projekt, (n.d.). http://www.powertogas.info/power-to-gas/pilotprojekte-im-
573 ueberblick/audi-e-gas-projekt/ (accessed August 29, 2018).

574 [13] Hydrogen energy storage: power ramp-up at the MYRTE test platform, (n.d.).
575 http://www.sa.areva.com/EN/news-10206/hydrogen-energy-storage-power-rampup-at-the-myrte-test-
576 platform.html (accessed August 29, 2018).

577 [14] M.-L. Charlot, B. Decourt, D. Ramard, C. Thébault, Gaz et énergies renouvelables, la bonne
578 combinaison pour un monde décarboné ?, Le journal de l'école de Paris du management. 120 (2016) 37–
579 44. doi:10.3917/jepam.120.0037.

580 [15] P. Panagiotopoulou, D.I. Kondarides, X.E. Verykios, Selective methanation of CO over supported
581 noble metal catalysts: Effects of the nature of the metallic phase on catalytic performance, Applied
582 Catalysis A: General. 344 (2008) 45–54. doi:10.1016/j.apcata.2008.03.039.

583 [16] C. de Leitenburg, A. Trovarelli, J. Kašpar, A Temperature-Programmed and Transient Kinetic
584 Study of CO_2 Activation and Methanation over CeO_2 Supported Noble Metals, Journal of Catalysis. 166
585 (1997) 98–107. doi:10.1006/jcat.1997.1498.

586 [17] M.A.A. Aziz, A.A. Jalil, S. Triwahyono, S.M. Sidik, Methanation of carbon dioxide on metal-
587 promoted mesostructured silica nanoparticles, Applied Catalysis A: General. 486 (2014) 115–122.
588 doi:10.1016/j.apcata.2014.08.022.

589 [18] Z. Kowalczyk, K. Stołecki, W. Raróg-Pilecka, E. Miśkiewicz, E. Wilczkowska, Z. Karpiński, Supported
590 ruthenium catalysts for selective methanation of carbon oxides at very low COx/H_2 ratios, Applied
591 Catalysis A: General. 342 (2008) 35–39. doi:10.1016/j.apcata.2007.12.040.

592 [19] C.H. Bartholomew, C.K. Vance, Effects of support on the kinetics of carbon hydrogenation on
593 nickel, Journal of Catalysis. 91 (1985) 78–84. doi:10.1016/0021-9517(85)90290-8.

594 [20] W. Wei, G. Jinlong, Methanation of carbon dioxide: an overview, Front. Chem. Sci. Eng. 5 (2010)
595 2–10. doi:10.1007/s11705-010-0528-3.

596 [21] G. Garbarino, D. Bellotti, E. Finocchio, L. Magistri, G. Busca, Methanation of carbon dioxide on
597 Ru/Al_2O_3: Catalytic activity and infrared study, Catalysis Today. 277, Part 1 (2016) 21–28.
598 doi:http://dx.doi.org/10.1016/j.cattod.2015.12.010.

[22] P. Ruterana, P.-A. Buffat, K.R. Thampi, M. Graetzel, The structure of ruthenium supported on titania: a catalyst for low-temperature methanation of carbon dioxide, Ultramicroscopy. 34 (1990) 66–72. doi:10.1016/0304-3991(90)90059-U.

[23] S. Tada, O.J. Ochieng, R. Kikuchi, T. Haneda, H. Kameyama, Promotion of CO_2 methanation activity and CH_4 selectivity at low temperatures over $Ru/CeO_2/Al_2O_3$ catalysts, International Journal of Hydrogen Energy. 39 (2014) 10090–10100. doi:10.1016/j.ijhydene.2014.04.133.

[24] H. Liu, S. Xu, G. Zhou, K. Xiong, Z. Jiao, S. Wang, CO_2 hydrogenation to methane over Co/KIT-6 catalysts: Effect of Co content, Fuel. 217 (2018) 570–576. doi:10.1016/j.fuel.2017.12.112.

[25] M. Agnelli, M. Kolb, C. Mirodatos, Co Hydrogenation on a Nickel Catalyst .: 1. Kinetics and Modeling of a Low-Temperature Sintering Process, Journal of Catalysis. 148 (1994) 9–21. doi:10.1006/jcat.1994.1180.

[26] S. Tada, T. Shimizu, H. Kameyama, T. Haneda, R. Kikuchi, Ni/CeO_2 catalysts with high CO_2 methanation activity and high CH_4 selectivity at low temperatures, International Journal of Hydrogen Energy. 37 (2012) 5527–5531. doi:10.1016/j.ijhydene.2011.12.122.

[27] G. Zhou, H. Liu, K. Cui, A. Jia, G. Hu, Z. Jiao, Y. Liu, X. Zhang, Role of surface Ni and Ce species of Ni/CeO_2 catalyst in CO_2 methanation, Applied Surface Science. 383 (2016) 248–252. doi:10.1016/j.apsusc.2016.04.180.

[28] S. Rahmani, M. Rezaei, F. Meshkani, Preparation of highly active nickel catalysts supported on mesoporous nanocrystalline γ-Al_2O_3 for CO_2 methanation, Journal of Industrial and Engineering Chemistry. 20 (2014) 1346–1352. doi:10.1016/j.jiec.2013.07.017.

[29] H. Muroyama, Y. Tsuda, T. Asakoshi, H. Masitah, T. Okanishi, T. Matsui, K. Eguchi, Carbon dioxide methanation over Ni catalysts supported on various metal oxides, Journal of Catalysis. (n.d.). doi:10.1016/j.jcat.2016.07.018.

[30] B. Mutz, H.W.P. Carvalho, S. Mangold, W. Kleist, J.-D. Grunwaldt, Methanation of CO_2: Structural response of a Ni-based catalyst under fluctuating reaction conditions unraveled by operando spectroscopy, Journal of Catalysis. 327 (2015) 48–53. doi:10.1016/j.jcat.2015.04.006.

[31] K. Zhao, W. Wang, Z. Li, Highly efficient Ni/ZrO_2 catalysts prepared via combustion method for CO_2 methanation, Journal of CO_2 Utilization. 16 (2016) 236–244. doi:10.1016/j.jcou.2016.07.010.

[32] F. Ocampo, B. Louis, A.-C. Roger, Methanation of carbon dioxide over nickel-based $Ce_{0.72}Zr_{0.28}O_2$ mixed oxide catalysts prepared by sol–gel method, Applied Catalysis A: General. 369 (2009) 90–96. doi:10.1016/j.apcata.2009.09.005.

[33] I. Graça, L.V. González, M.C. Bacariza, A. Fernandes, C. Henriques, J.M. Lopes, M.F. Ribeiro, CO_2 hydrogenation into CH_4 on NiHNaUSY zeolites, Applied Catalysis B: Environmental. 147 (2014) 101–110. doi:10.1016/j.apcatb.2013.08.010.

[34] K. Müller, M. Fleige, F. Rachow, D. Schmeißer, Sabatier based CO_2-methanation of Flue Gas Emitted by Conventional Power Plants, Energy Procedia. 40 (2013) 240–248. doi:10.1016/j.egypro.2013.08.028.

[35] J. Liu, C. Li, F. Wang, S. He, H. Chen, Y. Zhao, M. Wei, D. G. Evans, X. Duan, Enhanced low-temperature activity of CO_2 methanation over highly-dispersed Ni/TiO_2 catalyst, Catalysis Science & Technology. 3 (2013) 2627–2633. doi:10.1039/C3CY00355H.

[36] Q. Liu, B. Bian, J. Fan, J. Yang, Cobalt doped Ni based ordered mesoporous catalysts for CO_2 methanation with enhanced catalytic performance, International Journal of Hydrogen Energy. (2018). doi:10.1016/j.ijhydene.2018.01.132.

[37] A. Westermann, B. Azambre, M.C. Bacariza, I. Graça, M.F. Ribeiro, J.M. Lopes, C. Henriques, Insight into CO_2 methanation mechanism over NiUSY zeolites: An operando IR study, Applied Catalysis B: Environmental. 174–175 (2015) 120–125. doi:10.1016/j.apcatb.2015.02.026.

[38] A. Westermann, B. Azambre, M.C. Bacariza, I. Graça, M.F. Ribeiro, J.M. Lopes, C. Henriques, The promoting effect of Ce in the CO_2 methanation performances on NiUSY zeolite: A FTIR In Situ/Operando study, Catalysis Today. 283 (2017) 74–81. doi:10.1016/j.cattod.2016.02.031.

[39] A.C.W. Koh, L. Chen, W. Kee Leong, B.F.G. Johnson, T. Khimyak, J. Lin, Hydrogen or synthesis gas production via the partial oxidation of methane over supported nickel–cobalt catalysts, International Journal of Hydrogen Energy. 32 (2007) 725–730. doi:10.1016/j.ijhydene.2006.08.002.

[40] S. Tang, J. Lin, K.L. Tan, Partial oxidation of methane to syngas over Ni/MgO, Ni/CaO and Ni/CeO_2, Catalysis Letters. 51 (1998) 169–175. doi:10.1023/A:1019034412036.

[41] V.R. Choudhary, A.M. Rajput, B. Prabhakar, A.S. Mamman, Partial oxidation of methane to CO and H_2 over nickel and/or cobalt containing ZrO_2, ThO_2, UO_2, TiO_2 and SiO_2 catalysts, Fuel. 77 (1998) 1803–1807. doi:10.1016/S0016-2361(98)00072-6.

[42] F. Azzolina-Jury, Novel boehmite transformation into γ-alumina and preparation of efficient nickel base alumina porous extrudates for plasma-assisted CO2 methanation, Journal of Industrial and Engineering Chemistry. 71 (2019) 410-424. doi:10.1016/j.jiec.2018.11.053.

[43] A. RAWLE, BASIC PRINCIPLES OF PARTICLE SIZE ANALYSIS, (n.d.). http://www.rci.rutgers.edu/~moghe/PSD%20Basics.pdf (accessed September 3, 2018).

[44] J. Gao, Y. Wang, Y. Ping, D. Hu, G. Xu, F. Gu, F. Su, A thermodynamic analysis of methanation reactions of carbon oxides for the production of synthetic natural gas, RSC Advances. 2 (2012) 2358–2368. doi:10.1039/C2RA00632D.

[45] S. Sahebdelfar, M.T. Ravanchi, Carbon dioxide utilization for methane production: A thermodynamic analysis, Journal of Petroleum Science and Engineering. 134 (2015) 14–22. doi:http://dx.doi.org/10.1016/j.petrol.2015.07.015.

667 [46] C.S. Sharma, R. Hughes, The behaviour of an adiabatic fixed bed reactor for the oxidation of
668 carbon monoxide—II: Effect of perturbations, Chemical Engineering Science. 34 (1979) 625–634.
669 doi:10.1016/0009-2509(79)85107-6.

670 [47] A.N. Subbotin, B.S. Gudkov, V.I. Yakerson, Temperature hysteresis phenomena in heterogeneous
671 catalysis, Russ Chem Bull. 49 (2000) 1373–1379. doi:10.1007/BF02495080.

672 [48] A.L. Patterson, The Scherrer Formula for X-Ray Particle Size Determination, Phys. Rev. 56 (1939)
673 978–982. doi:10.1103/PhysRev.56.978.

674 [49] R. Daroughegi, F. Meshkani, M. Rezaei, Enhanced activity of CO_2 methanation over mesoporous
675 nanocrystalline Ni–Al_2O_3 catalysts prepared by ultrasound-assisted co-precipitation method,
676 International Journal of Hydrogen Energy. 42 (2017) 15115–15125. doi:10.1016/j.ijhydene.2017.04.244.

677 [50] G. Poncelet, M.A. Centeno, R. Molina, Characterization of reduced α-alumina-supported nickel
678 catalysts by spectroscopic and chemisorption measurements, Applied Catalysis A: General. 288 (2005)
679 232–242. doi:10.1016/j.apcata.2005.04.052.

680 [51] C. Li, Y.-W. Chen, Temperature-programmed-reduction studies of nickel oxide/alumina catalysts:
681 effects of the preparation method, Thermochimica Acta. 256 (1995) 457–465. doi:10.1016/0040-
682 6031(94)02177-P.

683 [52] L. Xu, X. Lian, M. Chen, Y. Cui, F. Wang, W. Li, B. Huang, CO_2 methanation over CoNi bimetal-
684 doped ordered mesoporous Al_2O_3 catalysts with enhanced low-temperature activities, International
685 Journal of Hydrogen Energy. 43 (2018) 17172–17184. doi:10.1016/j.ijhydene.2018.07.106.

686 [53] S. Tada, T. Shimizu, H. Kameyama, T. Haneda, R. Kikuchi, Ni/CeO_2 catalysts with high CO_2
687 methanation activity and high CH_4 selectivity at low temperatures, International Journal of Hydrogen
688 Energy. 37 (2012) 5527–5531. doi:10.1016/j.ijhydene.2011.12.122.

689 [54] R. Zhou, N. Rui, Z. Fan, C. Liu, Effect of the structure of Ni/TiO_2 catalyst on CO_2 methanation,
690 International Journal of Hydrogen Energy. 41 (2016) 22017–22025.
691 doi:http://dx.doi.org/10.1016/j.ijhydene.2016.08.093.

692 [55] M.A.A. Aziz, A.A. Jalil, S. Triwahyono, R.R. Mukti, Y.H. Taufiq-Yap, M.R. Sazegar, Highly active Ni-
693 promoted mesostructured silica nanoparticles for CO_2 methanation, Applied Catalysis B: Environmental.
694 147 (2014) 359–368. doi:10.1016/j.apcatb.2013.09.015.

695 [56] P.A.U. Aldana, F. Ocampo, K. Kobl, B. Louis, F. Thibault-Starzyk, M. Daturi, P. Bazin, S. Thomas,
696 A.C. Roger, Catalytic CO_2 valorization into CH_4 on Ni-based ceria-zirconia. Reaction mechanism by
697 operando IR spectroscopy, Catalysis Today. 215 (2013) 201–207. doi:10.1016/j.cattod.2013.02.019.

698 [57] T.A. Le, M.S. Kim, S.H. Lee, T.W. Kim, E.D. Park, CO and CO_2 methanation over supported Ni
699 catalysts, Catalysis Today. 293–294 (2017) 89–96. doi:10.1016/j.cattod.2016.12.036.

700 [58] G. Garbarino, D. Bellotti, P. Riani, L. Magistri, G. Busca, Methanation of carbon dioxide on
701 Ru/Al_2O_3 and Ni/Al_2O_3 catalysts at atmospheric pressure: Catalysts activation, behaviour and stability,
702 International Journal of Hydrogen Energy. 40 (2015) 9171–9182. doi:10.1016/j.ijhydene.2015.05.059.

703 [59] H. Liu, X. Zou, X. Wang, X. Lu, W. Ding, Effect of CeO_2 addition on Ni/Al_2O_3 catalysts for
704 methanation of carbon dioxide with hydrogen, Journal of Natural Gas Chemistry. 21 (2012) 703–707.
705 doi:10.1016/S1003-9953(11)60422-2.

706

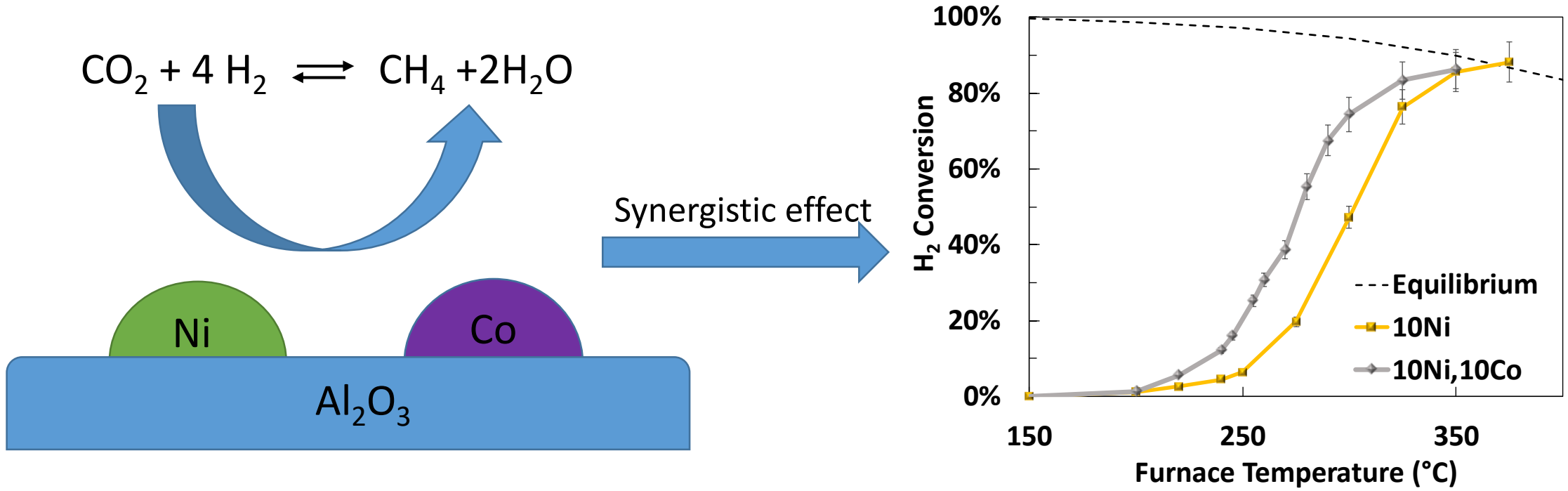
$CO_2 + 4\ H_2 \rightleftharpoons CH_4 + 2H_2O$
Ni
Co
Al_2O_3
Synergistic effect
100%
80%
60%
40%
20%
0%
H_2 Conversion
150
250
350
Furnace Temperature (°C)
Equilibrium
10Ni
10Ni,10Co